Tribology International 43 (2010) 929–934

Contents lists available at ScienceDirect

Tribology International

journal homepage: www.elsevier.com/locate/triboint

Microstructural and abrasive characteristics of high carbon Fe–Cr–C hardfacing alloy

Chia-Ming Chang, Yen-Chun Chen, Weite Wu *

Department of Materials Science and Engineering, National Chung Hsing University, Taiwan

ARTICLE INFO

Available online 24 December 2009

Keywords:
Metal matrix composite
Abrasive wear
Hard coating

ABSTRACT

A series of high carbon Fe–Cr–C hardfacing alloys were produced by gas tungsten arc welding (GTAW). Chromium and graphite alloy fillers were used to deposit hardfacing alloys on ASTM A36 steel substrates. Depending on the four different graphite additions in these alloy fillers, this research produced hypereutectic microstructures of Fe–Cr phase and $(Cr,Fe)_7C_3$ carbides on hard-facing alloys. The microstructural results indicated that primary $(Cr,Fe)_7C_3$ carbides and eutectic colonies of [Cr–Fe+$(Cr,Fe)_7C_3$] existed in hardfacing alloys. With increasing the C contents of the hardfacing alloys, the fraction of primary $(Cr,Fe)_7C_3$ carbides increased and their size decreased. The hardness of hardfacing alloys increased with fraction of primary $(Cr.Fe)_7C_3$ carbides. Regarding the abrasive characteristics, the wear resistance of hardfacing alloys were related to the fraction of primary $(Cr,Fe)_7C_3$ carbides. The wear mechanism was also dominated by the fraction of primary $(Cr,Fe)_7C_3$ carbides. Fewer primary carbides resulted in continuous scratches worn on the surface of hardfacing alloy. In addition, the formation of craters resulted from the fracture of carbides. However, the scratches became discontinuous with increasing fraction of the carbides. More primary carbides can effectively prevent the eutectic colonies from the damage of abrasive particles.

1. Introduction

Fe–Cr–C alloys are widely used in severe abrasive conditions due to their superior abrasion resistance. The excellent abrasive wear resistance results from high volume fraction of carbides and the toughness of the matrix also contribute to the wear resistance [1]. Properties such as abrasion wear resistance, surface roughening resistance and seizing or sticking resistance are essentially significant to these alloyed white cast irons used for the rolls and other wear resistant parts of steel rolling and mineral pulverizing mills. Among these properties, the abrasion wear resistance is reported to be dependent upon not only type, morphology, amount, and distribution pattern of the carbides precipitated from the melt, but also the type of matrix structure [2].

$(Cr,Fe)_7C_3$ carbides are found in Fe–Cr–C alloys with higher contents of carbon (2–5 wt%) and chromium (18–30 wt%). These microstructures indicate good wear resistance properties. These kinds of hard material can be represented by high Cr white cast iron which has high hardness M_7C_3 (about 1600 HV) [3–6]. Cr_7C_3 is well known for its excellent combination of high hardness, excellent wear resistance as well as good corrosion and oxidation resistance, so it has been widely used as the reinforcing phase in the composite coatings [7–10]. The $(Cr,Fe)_7C_3$ carbide reinforces composite coating has an excellent wear resistance. First, with the high hardness, the proeutectic $(Cr,Fe)_7C_3$ carbides can successfully retard plastic deformation when interacting with the counter surface during the sliding wear process. Therefore, the effect of adhesive deformation on material removal rate is low.

High-energy density sources have been widely applied in the hardfacing alloys to enhance wear and corrosion resistance of materials surface, such as electron beam, plasma arc, and laser [11–13]. The gas tungsten arc welding (GTAW) process (also called TIG welding) is used when a good weld appearance and high quality weld are required. In this process, an electric arc forms between a tungsten electrode and a base metal. The arc region is protected by a kind of inert gas or a mixture of inert gases. Electrons emit from the tungsten electrode and accelerate while traveling through the arc. A significant amount of energy, called the work function, is required for an electron to be emitted from the electrode. When the electron enters the workpiece, an amount of energy equivalent to the work function is released to melt the filler and base metal.

The purpose of this study is to investigate the effect of carbon addition on microstructure and abrasive property in the hypereutectic Fe–Cr–C alloy. Therefore, a series of high carbon Fe–Cr–C hardfacing alloys are produced by gas tungsten arc welding in this study. The abrasive characteristics of hardfacing alloys with different carbon contents are discussed from the observation of microstructural variation.

* Corresponding author.
E-mail address: wwu@dragon.nchu.edu.tw (W. Wu).

0301-679X/$ - see front matter © 2009 Elsevier Ltd. All rights reserved.
doi:10.1016/j.triboint.2009.12.045

Table 1
Alloy filler components.

	Graphite (wt%)	Chromium (wt%)
Specimen A	10	90
Specimen B	15	85
Specimen C	20	80

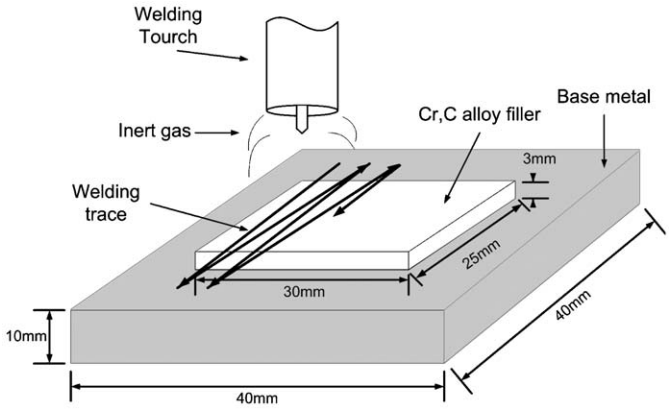

Fig. 1. Schematic diagram of the hardfacing welding.

Table 2
GTAW operating parameters.

Parameter	Value
Electrode	
Type	W-2%ThO
Diameter	3.2 mm
Angle	45°
Voltage	15 V
Current	200 A
Protective Gas	
Type	Ar
Flow	15 l/mm
Welding speed	
Travel speed	30 mm/min
Oscillate speed	300 mm/min

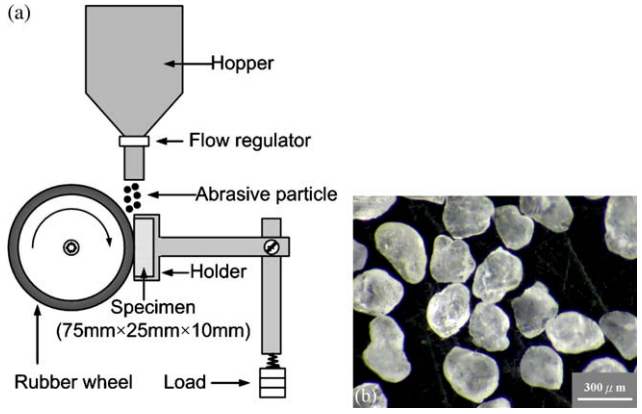

Fig. 2. Abrasive wear tests: (a) Schematic of the dry sand–rubber wheel testing machine, (b) Morphology of quartz particles used in abrasion tests.

Table 3
Abrasive wear test conditions, dry sand–rubber wheel testing machine.

Parameter	Value
Condition	
Wheel revolutions	6000
Velocity	200 rpm
Load	130 N
Sand flow	300 g/min
Abrasive particles	
Nature	Quartz
Size	200–300 μm
Hardness	1000–1100 HV

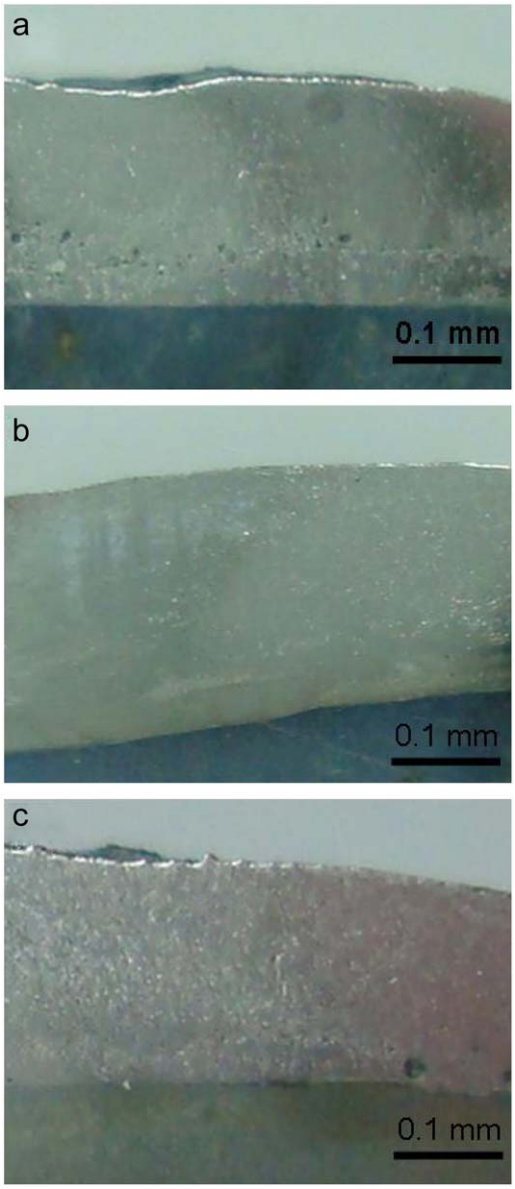

Fig. 3. Cross-sectional micrographs of hardfacing alloys with different C contents: (a) 3.61 wt%, (b) 4.47 wt% and (c) 5.21 wt%.

2. Experimental details

Base metals (150 mm × 100 mm × 10 mm) for the welding surface were prepared from ASTM A36 steel plates. Before welding, these specimens were ground and cleaned with acetone.

To obtain a series of high carbon hypereutectic Fe–Cr–C hardfacing alloys, the experiment mixed together various amounts of graphite and chromium powders. Table 1 illustrates the alloy filler components. Then, the different fillers with compact alloy powder were prepared by a constant high pressure of 1500 psi (105.39 kg cm^{-2}), so as to form alloy filler with dimension of 30 mm × 25 mm × 3 mm.

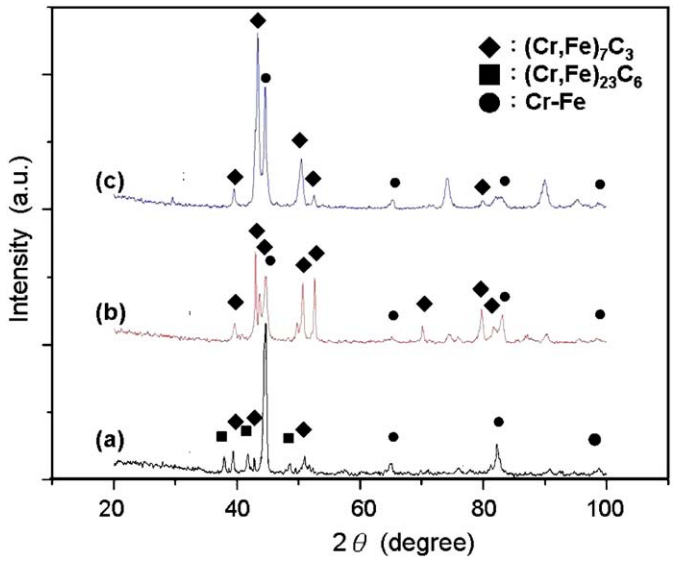

Fig. 4. X-ray spectrum of hardfacing alloys with different carbon contents: (a) 3.61 wt%, (b) 4.47 wt% and (c) 5.21 wt%.

Table 4
Chemical compositions of specimens by OES.

Specimen	C	Cr	Mn	Si	Fe
Low C content (A)	3.61	33.86	0.18	0.48	bal.
Medium C content (B)	4.47	30.72	0.22	0.37	bal.
High C content (C)	5.21	30.78	0.14	0.34	bal.

Bead-on-plate with oscillation GTAW was carried out with an electric power supply using an auto-mechanized system in which the welding torch was moved back and forth at a constant speed above the alloy filler. The GTA process melted the base metal and alloy filler to produce hardfacing alloy. Fig. 1 shows the schematic diagram of the welding method, while Table 2 presents the range of welding conditions in this study.

The experiment utilized an optical emission spectrograph (OES) to analyze chemical composition of the hardfacing alloys. X-ray diffraction (XRD) specimens were prepared from the top surface of the hardfacing, and X-ray diffraction with Cu Kα radiation was used to analyze the constituent phases. The hardfacing alloy structures were examined by optical microscopy (OM). Microstructural observations were carried out on the top surface of the hardfacing, after polishing and etching. The etching agent was composed of 20 g ammonium hydrogen fluoride, 0.5 g potassium pyrosulfite, and 100 ml H_2O at 80 °C. The whole hardness was taken on the top surface of the hardfacing alloys by the Rockwell hardness tester (C scale).

Abrasive wear test was performed in a dry sand–rubber wheel testing machine (Fig. 2a) according to ASTM G65 standard. Rounded quartz particles with mean diameter between 200 and 300 μm were used (Fig. 2b). The parameter of the abrasive wear test was shown in Table 3 for each hardfacing tested. After wear test, the observation of worn surface was examined by a scanning electron microscope (SEM).

3. Results and discussion

GTAW surface modification by means of alloying was the process by which chromium and graphite alloy filler of desirable compositions and a thin surface layer of the base metal were simultaneously melted and then rapidly solidified to form a dense coating bonded to the base metal. Because the substrate material was carbon steel besides chromium and carbon, the hardfacing layer also had iron to form Fe–Cr–C alloys. Fig. 3 shows cross-sectional micrographs of the hardfacing alloy. The thickness of the hardfacing with different carbon additions ranged from 2 to 3 mm. The melted surface gave a smooth rippled surface topography.

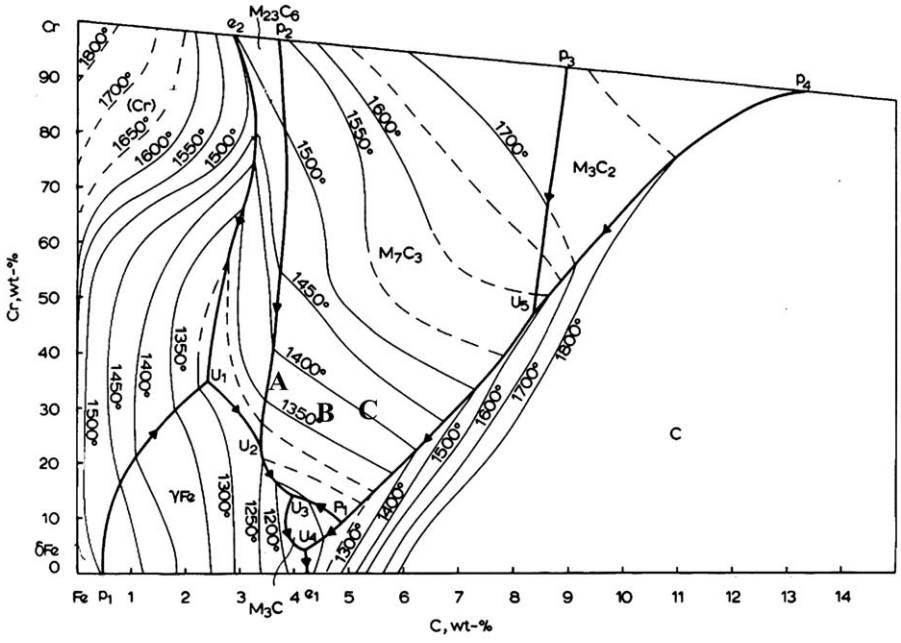

Fig. 5. Liquidus projection of the Fe–Cr–C ternary system.

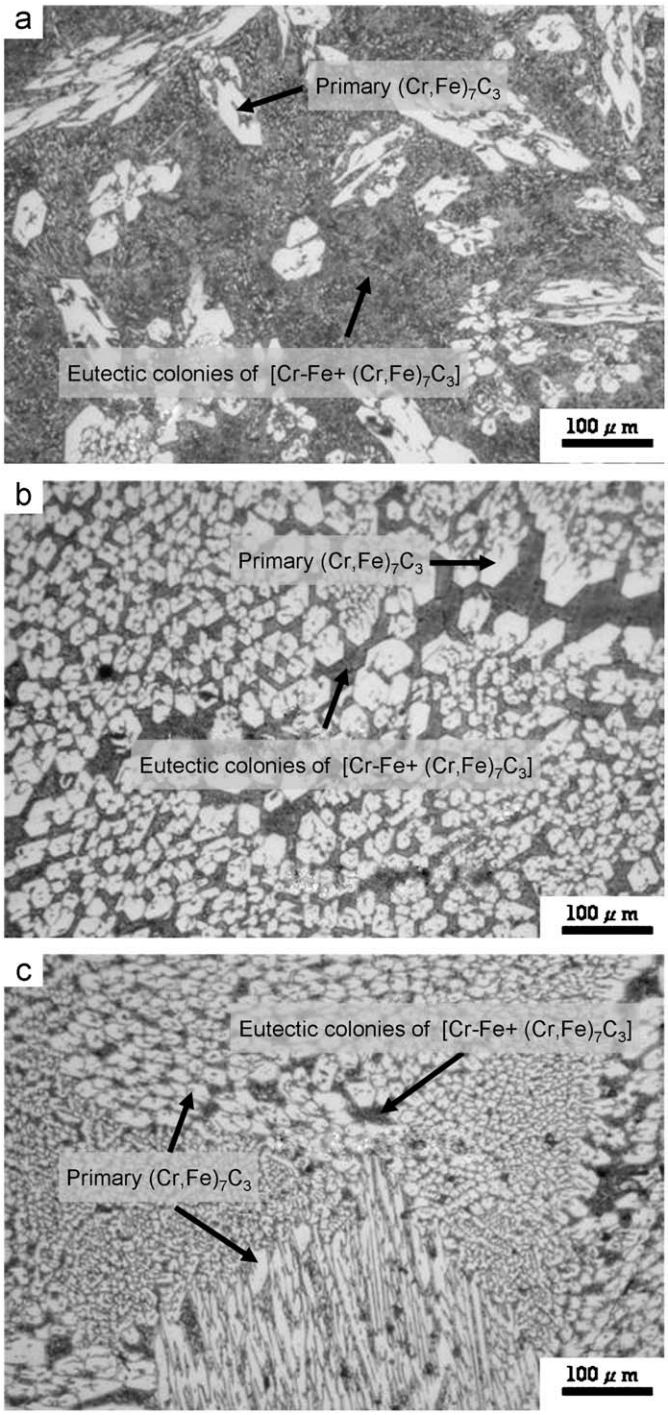

Fig. 6. Optical micrographs of hardfacing alloys with different C contents: (a) 3.61 wt%, (b) 4.47 wt% and (c) 5.21 wt%.

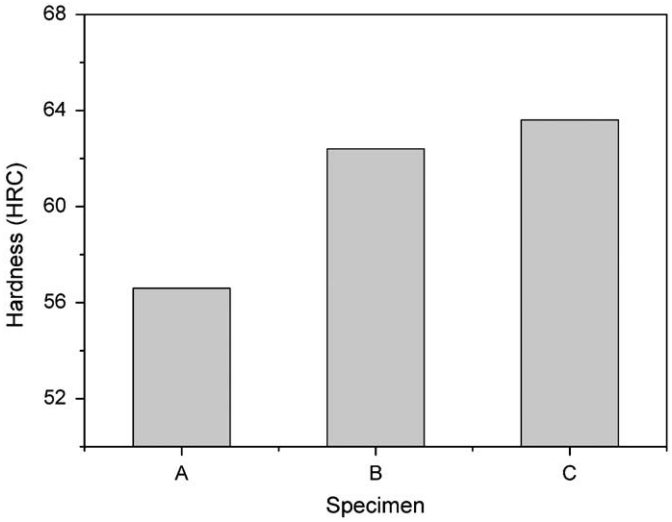

Fig. 7. Hardness of hardfacing alloys with different C contents.

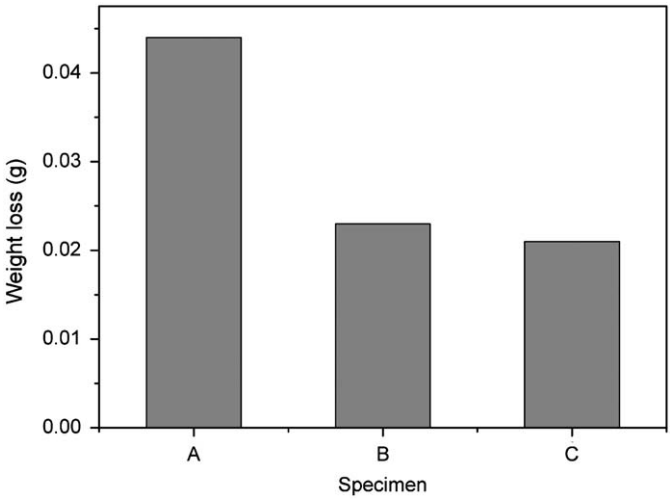

Fig. 8. Wear loss of hardfacing alloys with different C contents.

Fig. 4 shows the XRD spectra of the hardfacing alloys. The phases in the low C alloy (Specimen A) consisted of Cr–Fe solid solution (α), $(Cr,Fe)_{23}C_6$ carbide with an complex f.c.c. crystal structure, and $(Cr,Fe)_7C_3$ carbide with hexagonal structure. The phases in medium and high C alloys (Specimens B and C, respectively,) comprised Cr–Fe and $(Cr,Fe)_7C_3$.

Table 4 lists the chemical compositions of hardfacing alloys, marked in liquidus projection for the Fe–Cr–C ternary system (Fig. 5) [14–16]. It was found that each hardfacing alloy lay in M_7C_3 region. Therefore, the primary phase was M_7C_3 during the solidification process. In addition, in high carbon Fe–Cr–C alloy, as the carbon content increased, the $(Cr,Fe)_{23}C_6$ carbides disappeared because $(Cr,Fe)_{23}C_6$ carbide was unstable for a high carbon content.

The effects of different graphite additions in the alloy filler on the hardfacing microstructure could be seen in Fig. 6 through optical microscopy. During solidification process, the primary $(Cr,Fe)_7C_3$ carbides formed, followed by the eutectic reaction [$L \rightarrow Cr–Fe+(Cr,Fe)_7C_3$]. Consequently, the primary $(Cr,Fe)_7C_3$ carbides and eutectic colonies of $Cr–Fe+(Cr,Fe)_7C_3$ were obtained in all hardfacing alloys. Moreover, the fraction of primary $(Cr,Fe)_7C_3$ carbides increased as the addition of graphite increased from 10 to 20 wt%, but that of eutectic colonies of $Cr–Fe+(Cr,Fe)_7C_3$ decreased. The addition of graphite could increase the driving force for the formation of carbides.

Furthermore, the size of primary $(Cr,Fe)_7C_3$ carbides decreased with carbon contents. The carbon addition led to the increase in nucleation rate of primary $(Cr,Fe)_7C_3$ carbide increasing. During solidification, the formation of primary $(Cr,Fe)_7C_3$ carbide released the latent heat caused the reduction of undercooling [20]. The more proeutectic $(Cr,Fe)_7C_3$ carbides formed, the more solidification latent heat was released. The undercooling of solid–liquid interface decreased because the solidification latent heat was released. The growth of primary $(Cr,Fe)_7C_3$ carbides was suppressed as the undercooling of solid–liquid interface decreased.

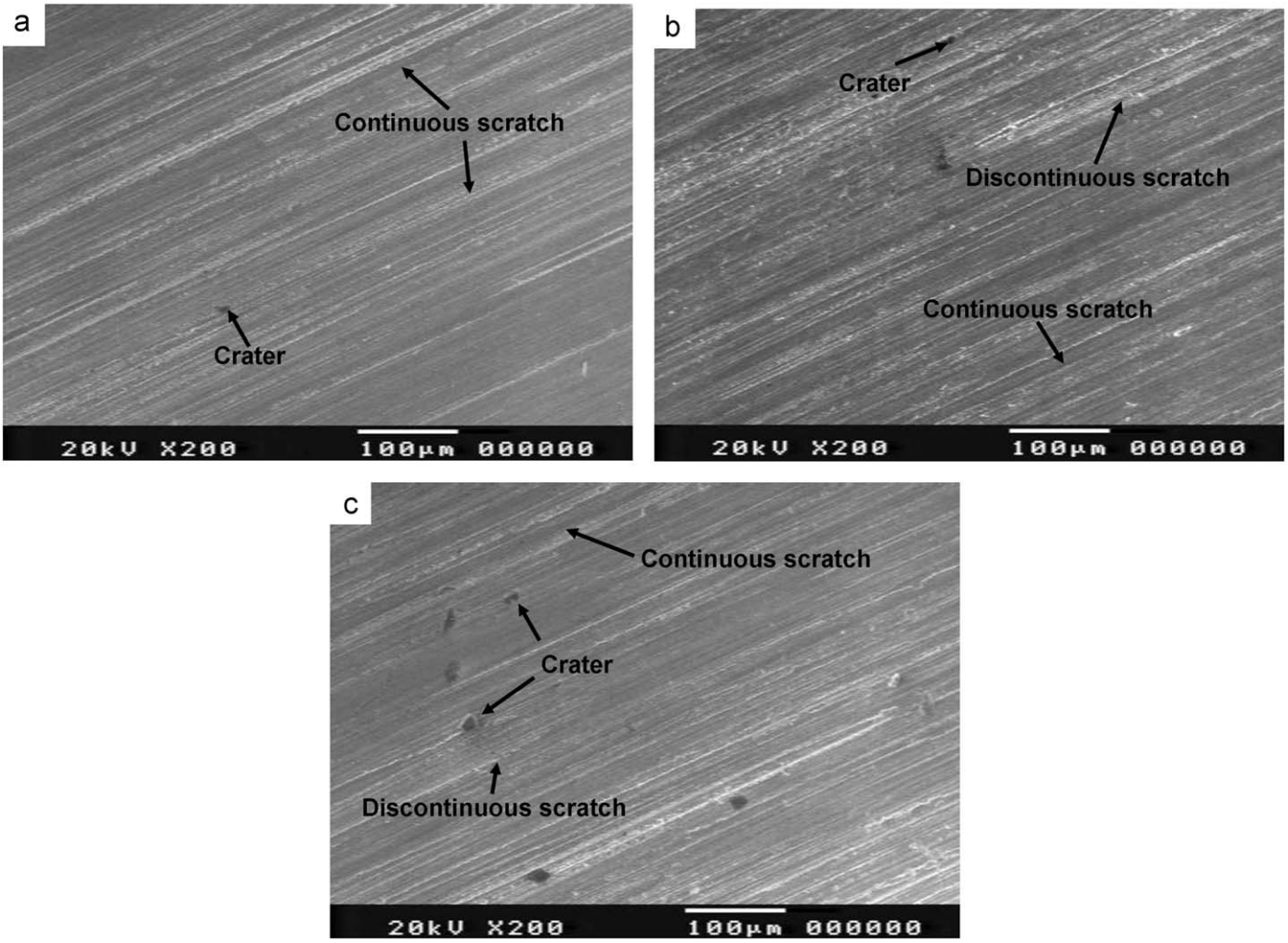

Fig. 9. Worn surfaces of hardfacing alloys with different C contents: (a) 3.61 wt%, (b) 4.47 wt% and (c) 5.21 wt%.

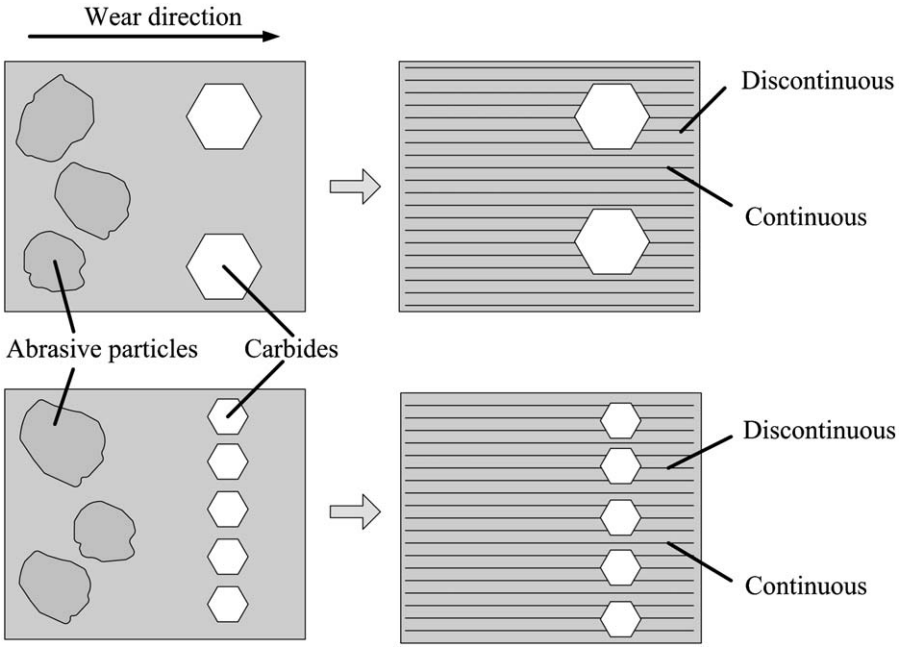

Fig. 10. Schematic diagram of the abrasive wear behavior.

Consequently, the size of primary $(Cr,Fe)_7C_3$ carbides decreased when the carbon content of hardfacing alloys increased.

The hardness of hardfacing alloys with different carbon contents is shown in Fig. 7. When addition of graphite increased from 10 to 20 wt%, the hardness increased from HRC 57 to HRC 64. More hard $(Cr,Fe)_7C_3$ carbides contributed to higher hardness of hardfacing alloy. The size of primary $(Cr,Fe)_7C_3$ carbides also enhanced the higher hardness according to the Hall–Petch relationship. Hence, the improvement of hardness was affected by the fraction and size of primary $(Cr,Fe)_7C_3$ carbides in current study.

Generally, the resistance of abrasive wear was related to the hardness of materials. Fig. 8 shows wear loss of hardfacing alloys with different C contents. This indicates that the wear loss decreased when C content increased. More primary carbides could prevent the eutectic colonies from the damage of abrasive particle. Therefore, the increasing carbon content could improve wear resistance of Fe–Cr–C alloy.

The observation of worn surface after abrasive wear test is shown in the Fig. 9, which suggests that scratches caused by abrasive particles became gradually shallower with the carbon content of Fe–Cr–C alloy. The hardness of primary $(Cr,Fe)_7C_3$ (about 1600 HV) is higher than the quartz (1000–1100 HV), thus primary $(Cr,Fe)_7C_3$ could effectively resist the damage of abrasive particle. Hence, more $(Cr,Fe)_7C_3$ carbides led to discontinuous scratches. In addition, craters were also found on the worn surface. The formation of craters is attributed to fracture of carbides. Hence, the craters increased with the fraction of primary carbides.

Fig. 10 illustrates schematically the abrasive wear behavior. In this study, the wear behavior was classified according to the morphology of scratches caused by abrasive particle. When the fraction of $(Cr,Fe)_7C_3$ carbides increased, the scratches were fewer. Furthermore, the scratches became discontinuous when the fraction of $(Cr,Fe)_7C_3$ increased. The discontinuous scratches formed because $(Cr,Fe)_7C_3$ impeded the damage of abrasive particles. Hence, more $(Cr,Fe)_7C_3$ caused the scratches to become shallower and discontinuous; and the wear loss of Fe–Cr–C alloy would decrease.

According to the above mentioned results, it could be concluded that the addition of graphite in the Fe–Cr–C alloys promoted the formation of hard $(Cr,Fe)_7C_3$ carbides. When the fraction of $(Cr,Fe)_7C_3$ increased, the hardness and wear resistance were enhanced. Therefore, the Fe–Cr–C alloy with high carbon content could be applied in severe abrasive conditions due to superior abrasion resistance.

4. Conclusion

This research used GTAW process to produce a series of Fe–Cr–C hypereutectic alloys. In this study, different graphite additions in the filler deposited the Fe–Cr–C hardfacing alloys with different carbon contents. The hypereutectic composite consisted of Cr–Fe solid solution (α), $(Cr,Fe)_7C_3$ carbide, and the trace amount of $(Cr,Fe)_{23}C_6$ carbide. The content and size of primary carbide and the fraction of eutectic colonies varied with different carbon contents. The hardness of hardfacing alloy increased with the carbon contents increased while the chromium carbide accompanied to refine. Regarding the wear characteristics, the wear resistance enhanced with the carbon contents. However, more primary carbides could prevent the eutectic matrix from the damage of abrasive particles. The scratches became discontinuous and shallow with increasing fraction of carbides. The formation of craters was attributed to the fracture of carbides. Therefore, high carbon hypereutectic Fe–Cr–C alloy possessed excellent wear resistance and could be applied in severe aggressive environments.

Acknowledgment

The authors are obligated to thank the National Science Council of Taiwan, ROC for its financial support under contracts of NSC-96-2221-E-005-054.

References

[1] Fan C, Chen MC, Chang CM, Wu W. Surf Coating and Technology 2006;201:908–12.
[2] Lu L, Soda H, McLean A. Materials Science and Engineering A 2003;347:214–22.
[3] Lin YC, Wang SW. Tribology International 2003;36:1–9.
[4] Svensson LE, Gretoft B, Ulander B, Bhadeshia HKDH. Journal of Material Science 1986;21:1015–9.
[5] Berns H, Fischer A. Materials Characterization 1997;39:499–527.
[6] Zhang AF, Xing JD, Fang L, Su JY. Wear 2004;257:198–204.
[7] Berns H. Wear 2003;254:47–54.
[8] Xing JD, Gao YM, Wang EZ, Bao CG. Wear 2002;252:755–60.
[9] Aso S, Goto S, Komatsu Y, Hartono W. Wear 2001;250:511–7.
[10] La PQ, Xue QJ, Liu WM. Wear 2001;249:93–9.
[11] Hou QY, Gao JS, Zhou F. Surface and Coatings Technology 2005;194:238–43.
[12] Wellman RG, Nicholls JR. Wear 2000;242:89–96.
[13] Eroglu M, Ozdemir N. Surface and Coatings Technology 2002;154:209–17.
[14] Raynor GV, Rivlin VG. Phase equilibria in iron ternary alloys. UK: The Institute of Metals, The Bath Press; 1988 pp. 143–155.
[15] Griffing NR, Forgeng WD, Healy GW. Transaction TMS-AIME 1962;224:148–59.
[16] Jackson RS. Journal of Iron Steel Institute 1970;208:163–7.